minerals

MDPI

Article

The Use of Stream Sediment Mineral Chemistry and U/Pb Geochronology for Regional Targeting: A Case Study from Yukon with Implications for Porphyry Cu and Orogenic Au Deposit Exploration

Ivan Belousov [1,2,*], Michael J. Baker [2], Leonid Danyushevsky [3] and Jeffrey Bigelow [4]

[1] CODES Analytical Laboratories, University of Tasmania, Hobart 7000, Australia
[2] Centre for Ore Deposit and Earth Sciences (CODES), University of Tasmania, Hobart 7000, Australia
[3] Friendly Solutions, Hobart 7000, Australia
[4] Newmont, Perth 6000, Australia
* Correspondence: ivan.belousov@utas.edu.au

Abstract

Stream sediments can provide extensive information about rocks from their catchments. Heavy mineral concentrates from stream sediments could be used during regional targeting when exploring for a range of different deposit types. Here, we present an example of using mineral chemistry coupled with U/Pb geochronology for zircons, titanites, and rutiles from a regional stream sediment study in Yukon with implications for porphyry Cu and orogenic Au deposit exploration in the region and globally. In this region, the location of the porphyry Cu deposit was determined based on rutile compositions, while an orogenic Au signature was identified primarily in titanite and rutile chemistry. The locations identified based on stream sediment mineral chemistry corresponded to the approximate locations of the Casino porphyry Cu and Coffee orogenic Au deposits. Other potential targets for follow-up exploration are also highlighted. This study accentuates that the addition of trace element mineral chemistry and U/Pb geochronology analyses to an exploration program provides substantial benefits in terms of constraining the ages of basement and host rocks and prioritising targets. The application of heavy mineral chemistry from stream sediments used for regional-scale targeting, followed by rock chip sampling and analysis at the camp scale, can provide significant exploration results, as demonstrated in this study.

Keywords: mineral chemistry; stream sediment; LA-ICP-MS; U/Pb geochronology; porphyry Cu; orogenic Au; metal exploration; Yukon; targeting

Check for updates

Academic Editor: Huan Li

Received: 20 December 2025
Revised: 20 February 2026
Accepted: 24 February 2026
Published: 26 February 2026

Copyright: © 2026 by the authors. Licensee MDPI, Basel, Switzerland. This article is an open access article distributed under the terms and conditions of the Creative Commons Attribution (CC BY) license.

1. Introduction

The distribution of resistant kimberlite indicator minerals in streams and sediments has been used as evidence for the proximity of the source of kimberlite for over a century [1]. Their compositions have been used extensively during diamond exploration for over 30 years, with particular interest in garnet [2–4], spinel [4,5], ilmenite [6], and pyroxenes [7]. The aforementioned minerals are quite resistant to weathering and can often be found in stream or till sediments. Consequently, analysing these mineral compositions from heavy mineral concentrates and finding signatures reflecting formation in a certain portion of the mantle and fast ascent to the surface have been used for targeting during exploration.

The use of stream sediments when exploring for other types of deposits was mostly limited to zircon U/Pb dating to identify regions of particular age known to host mineralisation in the area. Rapid development of analytical methods has made the dating of a much wider range of minerals (e.g., apatite [8], garnet [9], titanite [10], calcite [11], rutile [9,12], and micas [13]) possible using a range of isotopic systems (e.g., U/Pb, Lu/Hf, and Rb/Sr). Certain magmatic [14,15] and hydrothermal alteration [16–18] minerals also have distinct compositions that can be used to predict a potential for mineralisation. Some of these minerals are resistant to weathering and can be preserved in stream or till sediments. This feature is mostly used for porphyry Cu deposit exploration, where zircons formed at highly oxidised conditions are used to highlight regions of interest [19]. Other minerals may be used, particularly during exploration for various deposit types under cover [20–22].

This study formed part of the AMIRA P1202 project 'Far-field and near-mine footprints—finding and defining the next generation of Tier 1 ore deposits' that ran from 2018 to 2021. It was developed as a "blind test" site where the sponsor company (Newmont) supplied heavy mineral concentrates from stream sediment sampling, as well as altered coordinates of the samples. The aim of the project team was to apply different techniques, including those developed during the project, and determine the location of mineralisation within the area covered by the samples. Here, we will use the true coordinates of the samples and present our results, outlining prospective areas and showing the locations of known deposits. We will discuss how well the prospectivity signatures from different minerals align with the location of deposits.

2. Materials and Methods

2.1. Sample Description

Thirty-three stream sediment samples were used in this study (Table S1), each containing zircon pan separates, as well as porphyry indicator mineral (PIM) hand-picked grains. The samples cover a ~50 × 30 km catchment area (1500 km^2). A map of the region was supplied with colour fills representing different drainages (Figure 1). The study area was subdivided into three parts to make the description of potential prospective areas easier. Most samples contained zircon, rutile, and titanite; therefore, their compositions were used for targeting.

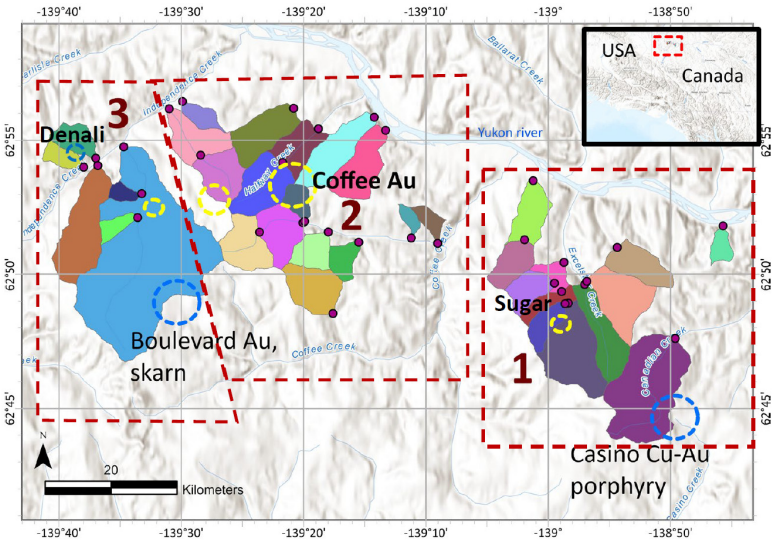


Figure 1. Map of the study area with the location of the samples (red symbols) and catchments coloured. Also shown are the locations of the Coffee Au project (several areas: yellow), as well as the Boulevard Au prospect and Toni Tiger skarn and Casino Cu–Au porphyry deposit (blue circles). Three areas (1, 2 and 3) are highlighted with dashed rectangles.

2.2. Methodology

Heavy mineral separates from each stream sediment sample were mounted in 1-inch epoxy mounts. The epoxy mount was dried for 12 h and polished using clean sandpaper and a clean polishing lap. The samples were then washed in distilled water in an ultrasonic bath. Prior to microanalysis, mounts were kept in a vacuum desiccator overnight to remove moisture and atmospheric air [23].

2.2.1. SEM

Each sample mount was mapped using the Bruker AMICS software package on the FEI MLA 650 ESEM (FEI, Hillsboro, OR, USA) instrument at the Central Science Laboratory, University of Tasmania. The system consists of fully automated energy-dispersive X-ray spectroscopy (EDS) that maps grain composition and matches with a database of over 2000 mineral phases.

Scanning electron microscopy was also used for the acquisition of backscatter electron (BSE) and cathodoluminescence (CL) images and was conducted at the Central Science Laboratory (CSL), University of Tasmania. Representative grains from each sample were BSE- or CL-imaged prior to analysis, with CL carried out for zircons and BSE for rutile and titanite. FEI MLA 650 ESEM, equipped with a Gatan PanaCLF panchromatic CL detector (Gatan Inc., Pleasanton, CA, USA), was used for zircon CL imaging, with a beam current and accelerating voltage of 2 $\pm$ 0.3 nA and 20 kV, respectively. Rutile and titanite BSE imaging was acquired simultaneously with microprobe analysis on a JEOL JXA-8530F Plus field emission electron microprobe (JEOL Ltd., Tokyo, Japan).

2.2.2. EPMA

A JEOL JXA-8530F Plus field emission electron microprobe equipped with 5 wavelength-dispersive spectrometers was used to acquire 321 analyses of titanites (30 samples) and 317 analyses of rutile (29 samples) at the Central Science Laboratory, University of Tasmania. EDS spectra were acquired and processed using a Thermo Pathfinder Pinnacle EDS system equipped with an UltraDry Extreme 30 mm^2 solid state detector (Thermo Fisher Scientific, Waltham, MA, USA). Electron microprobe analyses of rutile were carried out with an accelerating voltage of 20 kV, a beam current of 200 nA, and a beam size of 2 µm. Rutile were analysed for Al, Si, Ca, V, Cr, Mn, Fe, Cu, Zr, Nb, Mo, Sn, Ta, W, and Ti. Two standards were analysed: synthetic rutile from P&H Developments, UK, and Rutile R632, Sakena River, Madagascar.

Electron microprobe analyses of titanite were carried out with an accelerating voltage of 20 kV, a beam current of 200 nA, and a beam size of 5 µm. Titanites were analysed for Si, Ca, Ti, Na, Mg, Al, V, Cr, Mn, Fe, Sr, Y, Zr, Nb, La, Ce, Nd, Sm, Gd, Dy, Er, Yb, and F. Five standards were analysed: Titanite OLT1 from Otter Lake, Quebec, Titanite YILT, synthetic titanite from Memorial University, synthetic rutile from P&H Developments, UK, and Natural Wollastonite $CaSiO_3$, University of Tasmania.

2.2.3. LA-ICP-MS

Zircon, titanite, and rutile trace element analyses and U/Pb geochronology were performed by the Laser Ablation Inductively Coupled Plasma Mass Spectrometry (LA-ICP-MS) technique at the CODES Analytical Laboratories at the University of Tasmania, Australia. The analyses were performed with an ASI/Applied Spectra RESOLution S-155 ablation system (Applied Spectra, Inc., West Sacramento, CA, USA) with a Coherent Compex Pro 110 Ar-F excimer laser (Coherent, Inc., Saxonburg, PA, USA) operating at a 193 nm wavelength and a pulse width of 20 ns. The laser system was coupled with an Agilent 7900 quadrupole ICP-MS (Agilent Technologies, Santa Clara, CA, USA). The

sample ablation was performed in a He atmosphere flowing at 0.35 L/min and immediately combined with Ar flowing at 1.05 L/min. Small amounts of nitrogen (~2 mL/min N_2) were also added to increase sensitivity for heavy masses. The ICPMS was tuned to maximise sensitivity while maintaining a U/Th of ≈1.05 during a line scan (3 µm/s) ablation of the NIST612 glass. The production of molecular oxide species (i.e., $^{232}Th^{16}O/^{232}Th$) was maintained at levels below 0.2%, while doubly charged ion species production (i.e., $^{44}Ca^{++}/^{44}Ca^{+}$) was kept under 0.1% while ablating the line scan with a 40 µm beam at 10 Hz and 3.5 J/cm^2 laser beam fluence.

The analysis time for all minerals was 60 s, with the initial 30 s used to measure gas background with the laser turned off and the remaining 30 s of signal analysis with the laser switched on. A spot size of 30 µm and frequency of 5 Hz were used with laser beam fluence of 2.1 J/cm^2 for zircon and titanite and 5 J/cm^2 for rutile [9]. The masses analysed include ^{31}P, ^{49}Ti, ^{56}Fe, ^{89}Y, ^{91}Zr, ^{93}Nb, ^{139}La, ^{140}Ce, ^{141}Pr, ^{146}Nd, ^{147}Sm, ^{153}Eu, ^{157}Gd, ^{159}Tb, ^{163}Dy, ^{165}Ho, ^{166}Er, ^{169}Tm, ^{172}Yb, ^{175}Lu, ^{178}Hf, ^{181}Ta, ^{204}Pb, ^{206}Pb, ^{207}Pb, ^{208}Pb, ^{232}Th, ^{235}U, and ^{238}U for zircons; ^{24}Mg, ^{27}Al, ^{29}Si, ^{43}Ca, ^{49}Ti, ^{55}Mn, ^{57}Fe, ^{89}Y, ^{90}Zr, ^{93}Nb, ^{118}Sn, ^{140}Ce, ^{146}Nd, ^{147}Sm, ^{153}Eu, ^{157}Gd, ^{163}Dy, ^{166}Er, ^{172}Yb, ^{178}Hf, ^{181}Ta, ^{182}W, ^{202}Hg, ^{204}Pb, ^{206}Pb, ^{207}Pb, ^{208}Pb, ^{232}Th, ^{235}U, and ^{238}U for rutiles and ^{27}Al, ^{29}Si, ^{43}Ca, ^{49}Ti, ^{55}Mn, ^{56}Fe, ^{89}Y, ^{90}Zr, ^{93}Nb, ^{139}La, ^{140}Ce, ^{141}Pr, ^{146}Nd, ^{147}Sm, ^{153}Eu, ^{157}Gd, ^{159}Tb, ^{163}Dy, ^{165}Ho, ^{166}Er, ^{169}Tm, ^{172}Yb, ^{175}Lu, ^{178}Hf, ^{181}Ta, ^{202}Hg, ^{204}Pb, ^{206}Pb, ^{207}Pb, ^{208}Pb, ^{232}Th, ^{235}U, and ^{238}U for titanites. The sweep time was 0.25 s for zircon and titanite and 0.23 s for rutile, with longer counting time on U and Pb isotopes compared to the other elements.

The reported element abundances in zircon, rutile, and titanite were calibrated on the NIST610 glass using the values of [24], using secondary standard corrections based on the compositions of glasses BCR-2G and GSD-1G (GeoReM preferred values; http://georem.mpch-mainz.gwdg.de/, accessed on 24 November 2021). Quantification was performed using ^{91}Zr as the internal standard element for zircons, ^{49}Ti for rutile, and ^{43}Ca for titanite, normalising all measured cations to the oxide total of 100%. All standards were analysed in duplicate at the beginning and end, and every 60 min throughout the analytical session.

The downhole fractionation, instrument drift, and mass bias correction factors for Pb/U ratios in zircons were calculated using analyses of the 91500 zircon using values from [25]. For rutiles, long-term averages of TB-1 rutile [26] were used, while for titanite, 19686 titanite was used with unpublished values obtained by the ID-MC-ICPMS method at the University of Melbourne. The instrument drift and mass bias correction factors for the $^{207}Pb/^{206}Pb$ ratio and $^{207}Pb/^{206}Pb$-based ages were calculated using analyses of the NIST610 glass, using the Pb isotopic values of [27]. The calibration of the U/Pb ages for zircons was checked on analyses of the Temora zircon [28] and the Plešovice zircon [29] analysed throughout the analytical session and treated as unknowns. The calibration of the U/Pb ages for rutiles was checked on R10 rutile [30] and R19 rutile [31]. The calibration of the U/Pb ages for titanites was checked on 100606 titanite (432.02 +/− 0.64 Ma), FC-3 titanite [32], and Mt Dromedary titanite [33].

The laser data was processed using the LADR software package (Norris Scientific, version 1.1.8). Data reduction was performed by visually inspecting each analysis spectrum and screening out large variations or inclusions in the trace element chemistry to be not included in data integration. Data reduction used was based on the method outlined in detail in [8] and is based on [34], where common Pb correction is carried out on the calibration standard. Intervals in the laser spectrum were chosen based on the lowest common Pb content and to avoid other mineral phases. Systematic uncertainties were calculated according to [35].

Due to time constraints, only 30 zircon grains and a maximum of 30 titanite and rutile grains were analysed per sample. Some data filtering was applied prior to interpreting the results with the empirical criteria for clean analyses. (1) Filtering out zircon analyses with elevated La (>0.25 ppm) due to possible contamination with apatite/other inclusions or metamictisation: such analyses would decrease the prospectivity displayed in the Ce anomaly, even if La is not used in calculation. (2) Zircon grains with >30 ppm Ti were also removed due to possible contamination with titanite and rutile inclusions: such analyses would show elevated calculated temperatures based on Ti in zircon. (3) Removing discordant grains: when working with ages of individual grains (compared to igneous samples), it is easier to misinterpret possible Pb loss for younger grains and common Pb addition for older grains.

For rutile and titanite, we did not use grains with $^{207}Pb/^{206}Pb > 0.75$, as in those analyses, the age estimate depends strongly on the common Pb composition used for anchoring. In some cases, an analysis may be split into two or three intervals with different amounts of common Pb to help with constructing isochrons; however, for trace element contents, those analyses are combined. Age estimates were not calculated for individual grains but required several grains/analyses from a population to be present.

2.3. Mineral Chemistry Criteria

Zircon, in most cases, has a magmatic origin and is often used to determine U/Pb crystallisation ages as well as determine magma redox conditions using Ce and Eu contents [36–38]. The prospectivity of each grain in this study was determined using Ce and Eu anomalies following the calculations presented in [38]. It was shown for the Yerington porphyry Cu–Au deposit [39], higher values of Eu and Ce anomalies are required in some regions. Therefore, prospectivity criteria determined based on Yerington zircons were used. The estimation of oxygen fugacity using zircon chemistry (e.g., [40]) was not used due to ranges in a single age population often exceeding the range of published terrestrial values.

Rutile can be formed at both the magmatic stage and as a result of hydrothermal alteration [22]. However, it is mostly hydrothermal rutile that is useful for prospectivity analysis [12,16,41]. It has been shown that rutile prospectivity for porphyry Cu deposits could be determined based on elevated V, Sn, and W concentrations [12,16], while other deposit types are often characterised by elevated Sn, W, and Sb [41]. Orogenic Au deposits often have similar ranges for W and Sn compared to porphyry Cu deposits but could be distinguished based on higher As and Sb contents [12]. Rutile from pegmatites could be distinguished based on elevated Nb, Ta, and Sn [41]. Rutile can also be dated by the U/Pb method [9,12,31]. Antimony was not analysed in this study; therefore, we used a combination of V, Sn, and W contents to determine the prospectivity of different areas. While specific values might vary between terranes, deposit types, and sizes of deposits, we used criteria of Sn > 500 ppm, V > 2000 ppm, and W > 950 ppm to determine prospective catchments, which were determined based on probability plots of concentrations of a particular element within the dataset.

Titanite can also be formed at both the magmatic stage and by hydrothermal alteration [22,42,43]. It is often used to trace the origin of mafic enclaves in granites [44,45] and granite crystallisation processes [43,46]. The zirconium content in titanite can be used to calculate formation temperatures [47]; however, titanites often have zircon inclusions, and the data needs to be carefully screened. Titanite can also be dated by the U/Pb method [32,48–50] and can be used to trace several episodes of hydrothermal alteration at the deposit scale [51]. In some cases, several episodes of titanite growth can be observed in a single rock sample with a simple isotopic system of coexisting zircon [52]. There are very few studies identifying trace element signatures of titanites related to a particular deposit

type [53–55], and it also seems to change composition during metamorphism [42]. The prospectivity of titanites in this study was determined based on REE contents. While REE could be transported by hydrothermal fluids [56], their concentrations are generally much lower compared to silicate melts. Therefore, as an indication of prospective hydrothermal titanite, we used low HREE contents [54]. We used a criterion of Yb < 8 ppm, which was determined based on our unpublished data from the giant Golden Mile Orogenic Au and probability plot of Yb concentrations within the dataset and confirmed on the dataset from the giant Batu Hijau porphyry Cu deposit. Igneous titanites are known to have elevated LREE contents [42], while titanites from porphyry Cu deposits are characterised by elevated LREE/HREE [57]. Therefore, as an indication of prospective magmatic titanite, we used high LREE/HREE (La/Yb > 7) at moderate HREE (8 ppm < Yb < 200 ppm) to not include granitic compositions, which are abundant in the area. Such cutoffs are supported by our unpublished data from Ann Mason (Yerington) and Collahuasi porphyry Cu deposits and probability plots within the dataset. The unpublished data used was collected as part of the AMIRA P1202 project and will be published elsewhere when the confidentiality period expires.

3. Geology and Known Deposits/Occurrences in the Area

3.1. Casino Porphyry

The Casino deposit (Measured and Indicated resources are 2.49 billion tonnes at 0.14% copper, 0.18 g/t gold, and 1.5 g/t silver) is centred on an east–west elongated porphyry stock (Patton porphyry) that intrudes the Dawson Range Batholith and Yukon Tanana terrane country rocks [58] (Figure 2). The Patton porphyry (72–74 Ma) represents two or more episodes of dacite to rhyodacite intrusions. The intrusion of the stock caused the brecciation of both the intrusion and the surrounding country rocks. Hypogene mineralisation consists of pyrite, chalcopyrite, molybdenite, and minor huebnerite, and is concentrated in the phyllic zone along the inner side of a pyrite halo and is surrounded by weakly developed argillic and propylitic alteration. Mineralisation at Casino is dated as Late Cretaceous (75–74 Ma; [59]). It was recently shown that the Casino deposit could be identified based on the presence of sulfides [60] and tourmaline [61] in stream sediments, as well as hydrogeochemistry of the surface waters [62].

3.2. Coffee Au

Coffee deposit (resource estimate at 1,000,000 tonnes grading 2.01 g/t gold in the Measured category (60,000 oz Au) and 54,500,000 tonnes grading 1.19 g/t gold in the Indicated category (2,080,000 oz Au) is interpreted to represent a shallow-level structurally controlled orogenic gold deposit [64,65]. Mineralisation is concentrated in several zones, namely Supremo, Latte, Double Double, and Kona. Mineralised rocks at Coffee record a succession of biotite replacement, sericitisation, silicification, and carbonatisation events that overprint earlier Jurassic sericitic alteration. Invisible gold at the deposit is hosted in fine-grained arsenian pyrite, and the arsenian pyrite is disseminated through host rocks and localised breccias [66]. The mineralised brittle structures cut across all of the rock types, including the 99 Ma Coffee Creek granite [67]. The Coffee Au deposit most likely formed as part of a broader orogenic mineralisation event that affected this part of the Yukon–Tanana terrane between 96 and 92 Ma [65]. The age of magmatism is constrained to between 98 Ma and 107 Ma based on multiple individual zircon ages from the Coffee Creek pluton and coeval dykes, while age determinations from hydrothermal white mica constrain mineralisation to ca. 97 Ma [63].

The Sugar occurrence is a separate part of the Coffee Au deposit (Figures 1 and 2) and represents a cluster of structurally controlled, diamond drill-tested, mineralised Au

zones located approximately 21 km SE of the main Coffee deposit. Gold mineralisation is associated with disseminated sulfides in zones of silica flooding and with variably sheared veins of quartz-carbonate-arsenopyrite +/− pyrite +/− freibergite +/− stibnite +/− sphalerite [68]. Mineralisation at the Sugar occurrence appears broadly contemporaneous and may represent a more deeply exhumed part of the Coffee deposit with deeper-seated, higher-temperature alteration types and vein-controlled mineralisation.

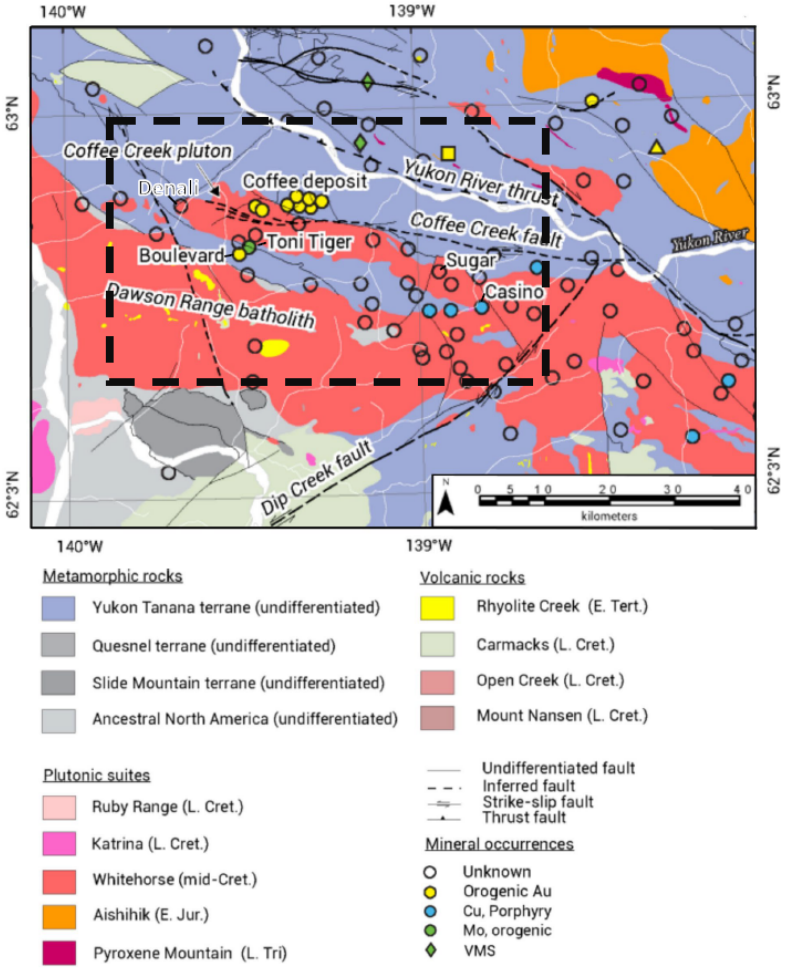


Figure 2. Simplified geologic map of the Dawson Range (modified after [63]) showing the distribution of mineral occurrences and deposits. The area from Figure 1 is highlighted with a dashed rectangle.

3.3. Boulevard Au Prospect and Toni Tiger Skarn Mo Anomaly

Boulevard and Toni Tiger are located next to each other: south of the headwaters of Independence Creek and ~10 km southwest of the Coffee Au deposit. Exploration work by Independence Gold at Boulevard (https://ingold.ca/project/yukon-properties/boulevard-project/, accessed on 25 May 2025) has identified 25 Au soil anomalies occurring in three main zones: Sunrise/Sunset and a separate Denali Zone (Figure 1). Gold mineralisation at the Sunrise/Sunset Zone appears to occur within north–northeast striking, steeply dipping structures with variable amounts of both sulfide minerals and vein quartz and is thought to be parallel to mineralised trends at Coffee. Gold mineralisation on the Boulevard prospect is hosted by quartzite, biotite chlorite schist and lesser chlorite biotite schist crosscut by quartz and quartz-carbonate veins with locally sericite-altered envelopes [67]. Mineralisation occurs as disseminated or massive arsenopyrite and stibnite with pyrrhotite occurring as disseminations and stringers outside of the main mineralisation zone. The area also contains the Toni Tiger Cu-Mo skarn, where mineralisation is hosted by quartz-garnet and quartz-molybdenite veins and comprises small blebs, stringers, and disseminations of

molybdenite, chalcopyrite, scheelite, pyrite, and arsenopyrite. The ages of mineralisation are ~95.9 Ma for Boulevard and ~95 Ma for Toni Tiger [67,69].

4. Results

4.1. Zircon

A total of 852 zircon grains were analysed from 33 samples, with 618 analyses left after initial filtering (Table S2). Zircon ages range from modern to Archean (0.1 to 2857 Ma; Figure 3a,b) with dominant age populations of ~110 Ma and ~260 Ma and less abundant populations at ~70 Ma, ~150 Ma, and ~340 Ma (Figure 3c). All age populations contain zircons that lie within the prospective porphyry field [37,38], with fewer grains classified into the prospective field based on a Ce anomaly relative to an Eu anomaly (see Discussion (Section 5); Figures 3 and 4). The distribution of prevalent age populations in zircons from stream sediments delineates general geologic boundaries in the area. We focused on the distribution of zircons from the most abundant populations (~110 and ~260 Ma) and the ~75 Ma population, corresponding to the age of the Casino porphyry deposit.

Most prospective zircons from the ~110 Ma age population clearly highlight the catchment of the Casino Cu-Au porphyry (Figure 5). Only one grain analysed in a sample from this catchment had a ~75 Ma age, with others mostly ~110 Ma; however, CL images reveal thin rims on most of the grains (Figure 6). Prospectivity of zircons from the ~110 Ma age population also highlights the catchment where the Boulevard Au prospect and Toni Tiger skarn deposit are located (Figure 5). The prospectivity of the ~260 Ma age population highlights catchments related to the Coffee Au deposit (Figure 5).

4.2. Rutile

A total of 324 rutile grains were analysed from 29 samples, with 308 analyses left after initial filtering (Table S3). Rutile U/Pb dating was not possible for all analyses due to very high common Pb ($^{207}Pb/^{206}Pb > 0.8$). However, ~75% of all rutile grains analysed have an age estimate, while for prospective grains, >90% have an age estimate. The majority of grains with age estimates form ~75 Ma and ~110 Ma age populations, with lesser populations at ~160–185 Ma and ~190–220 Ma, and a minor population at ~260 Ma (Figure 7a).

Tin. There were 20 analysed grains with Sn > 500 ppm, with five of them without age estimates. The majority of prospective grains had a ~75 Ma age (Figure 7b), with 90% of them coming from the catchment of the Casino porphyry deposit (Figure 8). That catchment is the most prospective, with 10 of 20 prospective grains based on Sn content; however, other areas also contain rutile with >500 ppm Sn, with three of them from the ~100 Ma population in the Coffee Au deposit catchment (Figure 8).

Vanadium. There were 70 rutile grains analysed with V > 2000 ppm, with only three of them without an age estimate. The most prospective grains were ~110 and ~75 Ma in age (Figure 7c); however, other age populations also contained rutile grains with V > 2000 ppm. Two of the areas with the most abundant grains with V > 2000 ppm were Area 3 (Figure 9) and had mostly ~110 Ma ages, with one of them potentially associated with the Denali Au occurrence. The catchment of the Casino porphyry deposit was the third-most prospective, with 10 of 70 grains having V > 2000 ppm.

Tungsten. There were 34 rutile grains analysed with W > 1000 ppm, with three of them without an age estimate. The most prospective grains with an age estimate were ~75 Ma (Figure 7d), with 93% (13 of 14) of them coming from the catchment of the Casino porphyry deposit. That catchment was the most prospective (Figure 8; 15 of 34 prospective rutile grains based on W content). However, other areas also contained rutile with >950 ppm

W, with most of them potentially associated with different zones of the Coffee Au deposit (Figure 9).

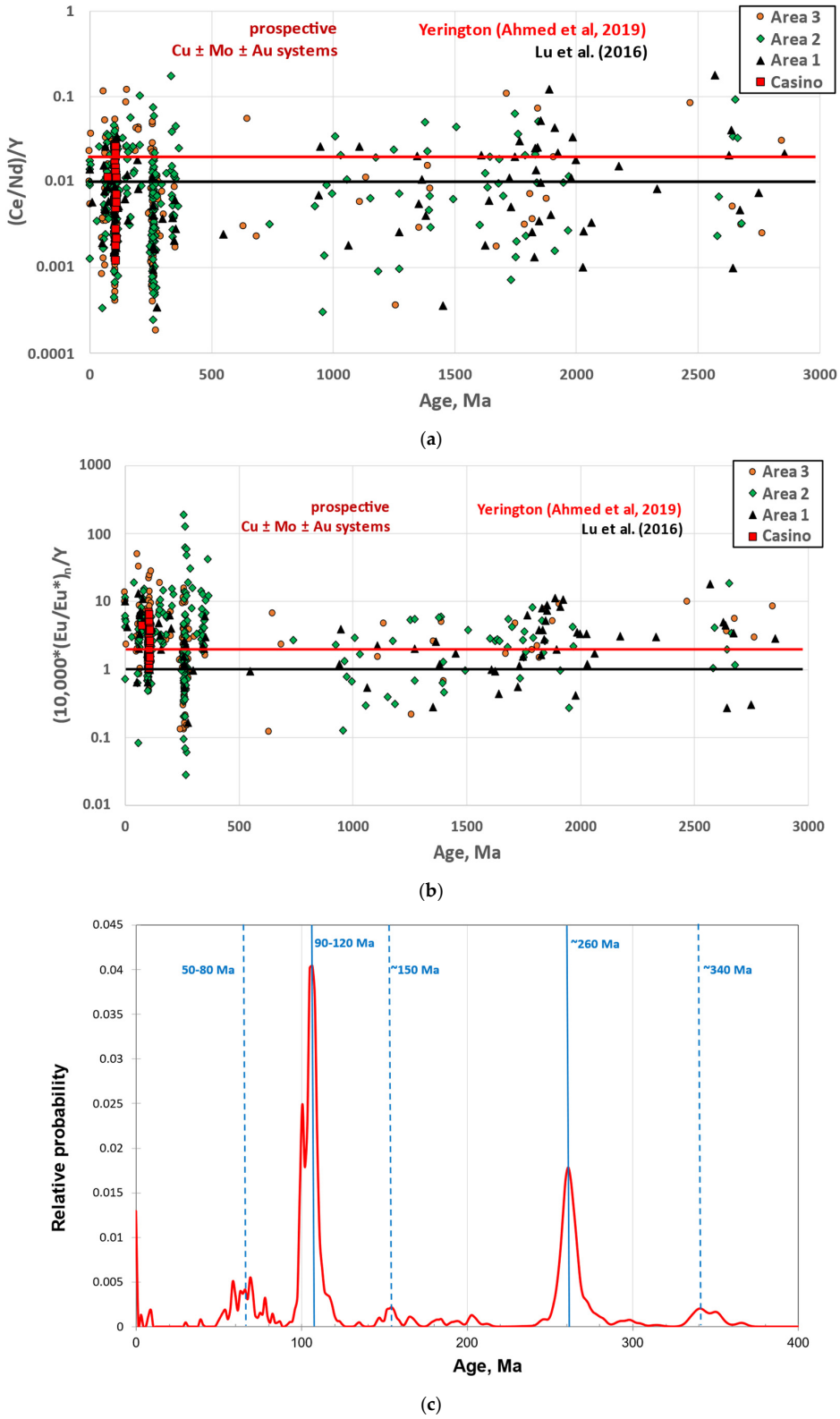


Figure 3. Variation in Ce (**a**) and Eu (**b**) anomalies as measures of zircon prospectivity with age. Prospectivity criteria are shown based on [38] (black line) and [39] (red line). Probability density plot (**c**) for zircons < 400 Ma from all samples combined. Eu* represents calculated value based on contents of neighboring REE.

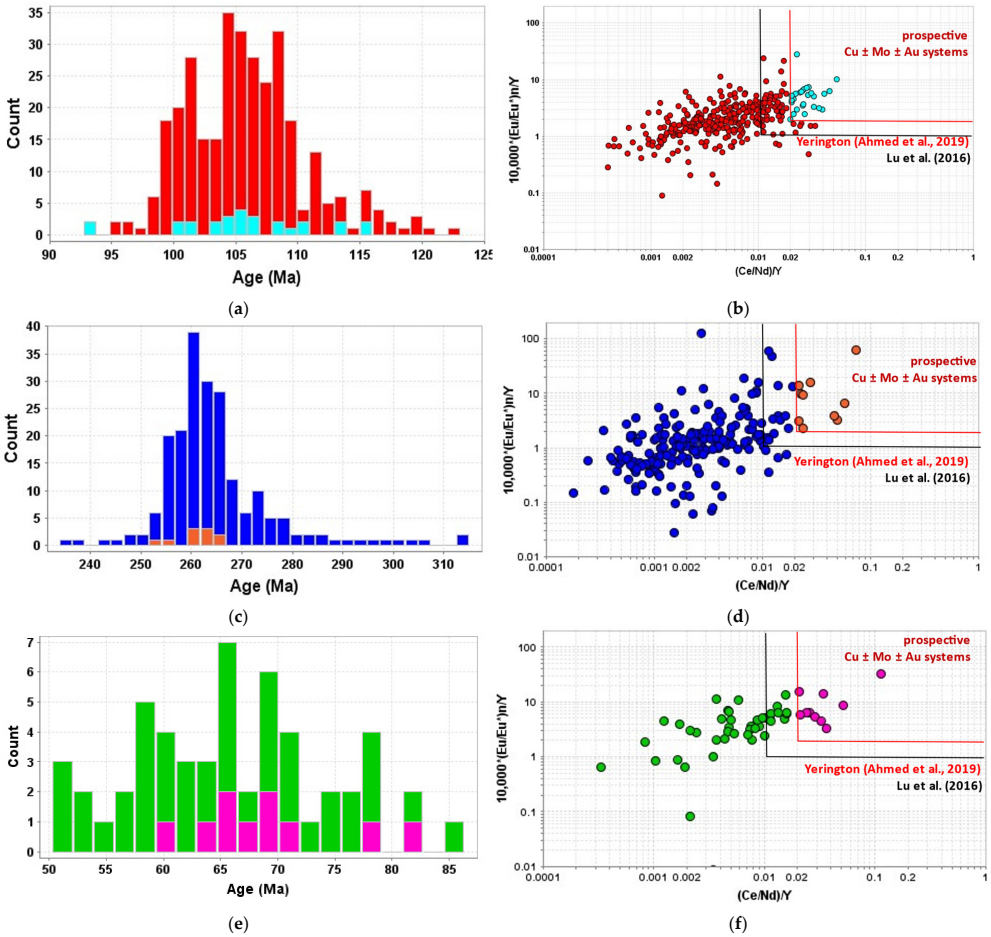


Figure 4. Distributions of zircon ages within ~110 Ma (**a**), ~260 Ma (**c**), and ~70 Ma (**e**) age groups and prospectivity of grains based on Ce and Eu anomalies (**b**,**d**,**f**) in zircon from respective age groups. Prospectivity criteria are shown based on [38] (black line) and [39] (red line). Eu* represents calculated value based on contents of neighboring REE. Different colours are used to highlight prospective grains on (**a**,**c**,**e**).

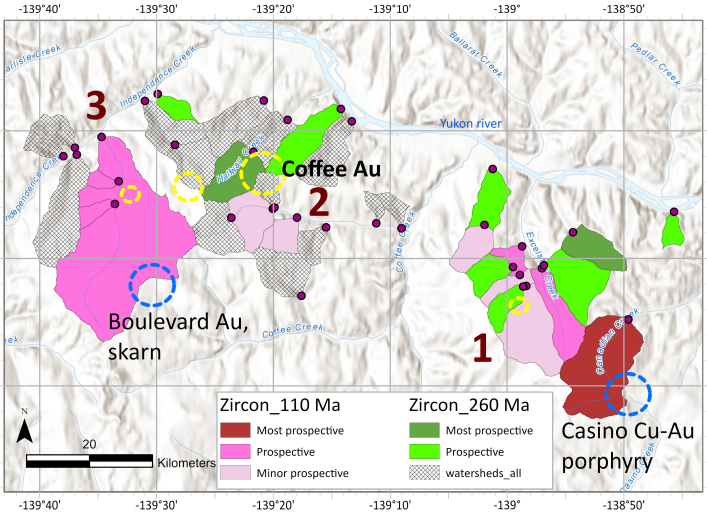


Figure 5. Catchments highlighted by zircon prospectivity. Only the most abundant zircon age populations (~110 Ma and ~260 Ma) are shown. Most prospective is defined by the highest number of prospective grains based on both Ce and Eu anomalies. Shaded catchments were sampled but not highlighted by prospectivity criteria. Other symbology from Figure 1.

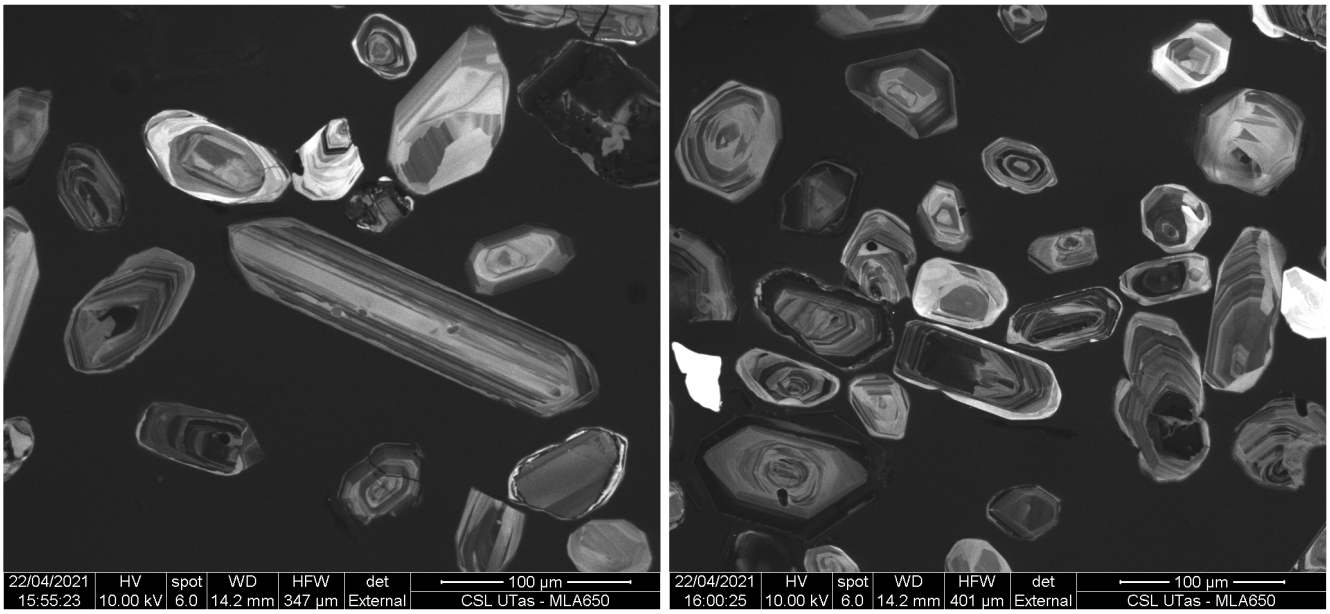


Figure 6. Cathodoluminescence (CL) images of zircons from a Casino porphyry deposit catchment sample showing the presence of thin rims too small to analyse separately on many grains.

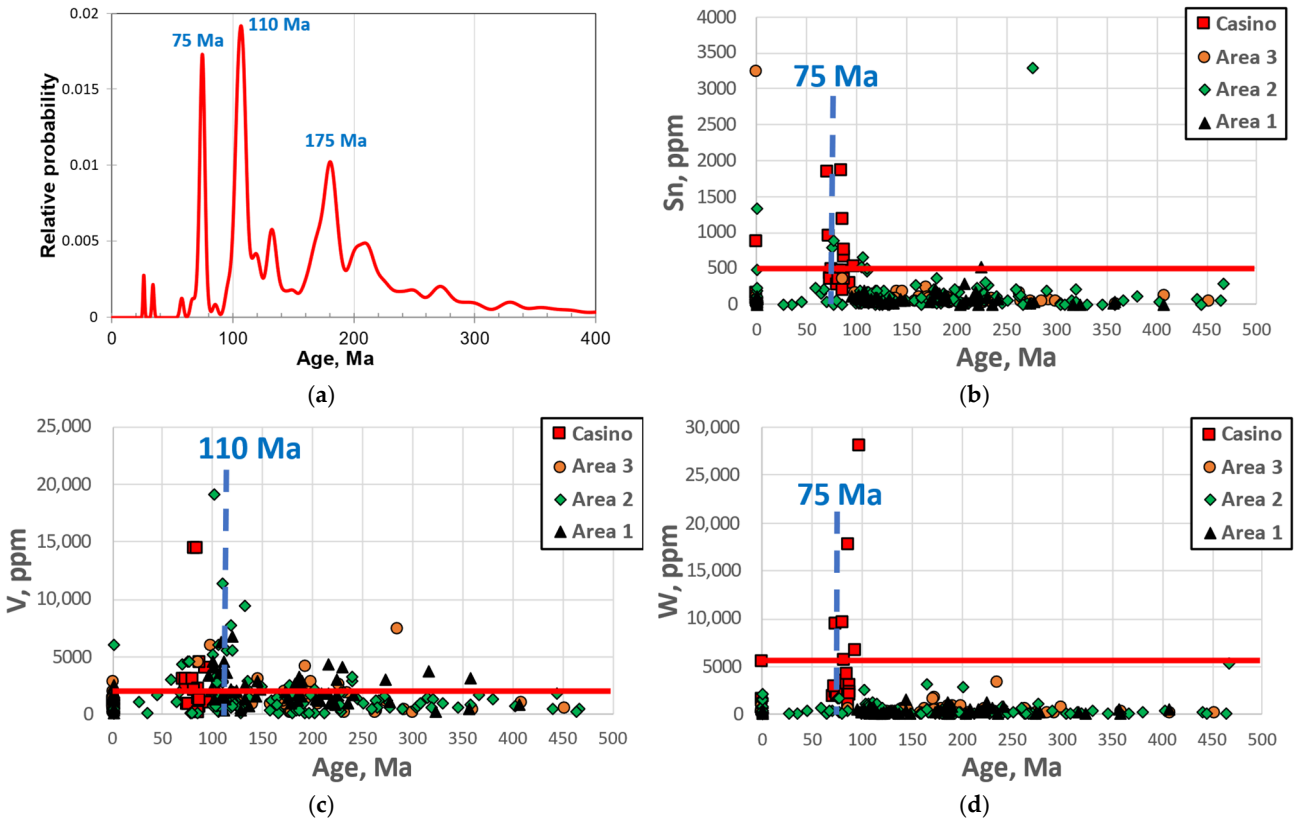


Figure 7. Probability density plot for datable rutiles from all samples with <400 Ma age estimates (**a**) and compositions of datable rutile with cutoffs for prospective grains: (**b**) Sn > 500 ppm, (**c**) V > 2000 ppm, and (**d**) W > 950 ppm. In (**b**–**d**), grains with no age estimate are shown to have 0 Ma age. Main age peak is highlighted with blue dashed line.

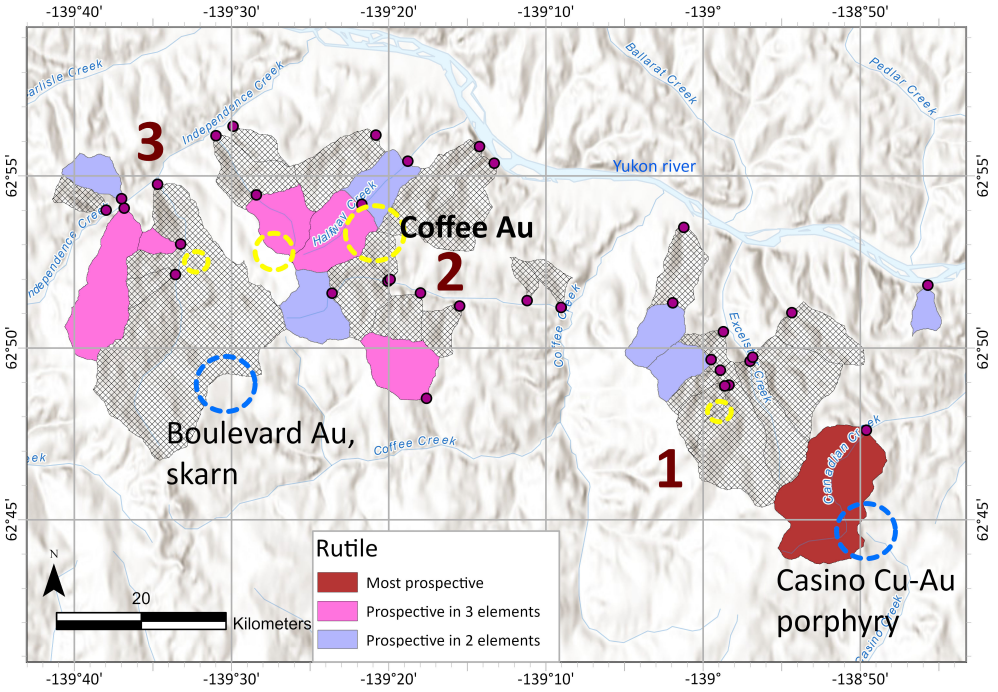


Figure 8. Map of the catchments with the highest number of prospective rutile grains. Shaded catchments were sampled but not highlighted by prospectivity criteria. Other symbology from Figure 1.

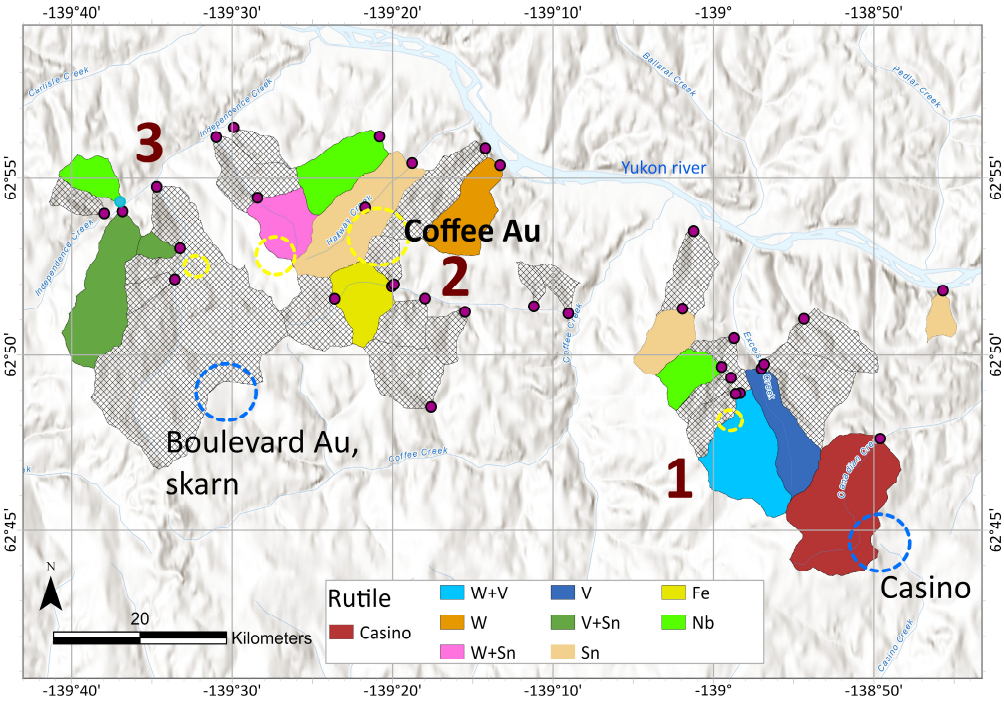


Figure 9. Map with catchments coloured based on rutile trace element prospectivity. Shaded catchments were sampled but not highlighted by prospectivity criteria. Other symbology from Figure 1.

Catchments adjacent to all ore deposits known in the area contain rutiles with anomalous trace element concentrations (Figure 8); however, trace element signatures differ between the deposits (Figure 9). The sample with the highest number of prospective analyses based on rutile Sn and W contents comes from catchment draining from the Casino Cu–Au porphyry (Figure 8). This sample is also characterised by rutiles, showing distinct

zonation in BSE images (Figure 10) with bright zones possibly reflecting high W contents. Several catchments of the Coffee Au deposit also contain rutiles with prospective chemistry (Figure 9). The most prospective catchments based on rutile V contents are in Area 3, with one of them potentially associated with the Denali Au occurrence. Different trace element signatures relate to different ages: high V contents are mostly in ~110 Ma age population rutiles, while high Sn and W rutiles are mainly ~75 Ma in age (Figure 7), most of which come from a sample within the Casino porphyry deposit catchment. U/Pb dating of rutiles from this catchment (Figure 11) exactly reproduces the age of this deposit [59]. There are also several catchments with anomalous Nb contents (Figure 9), which might be prospective for pegmatites.

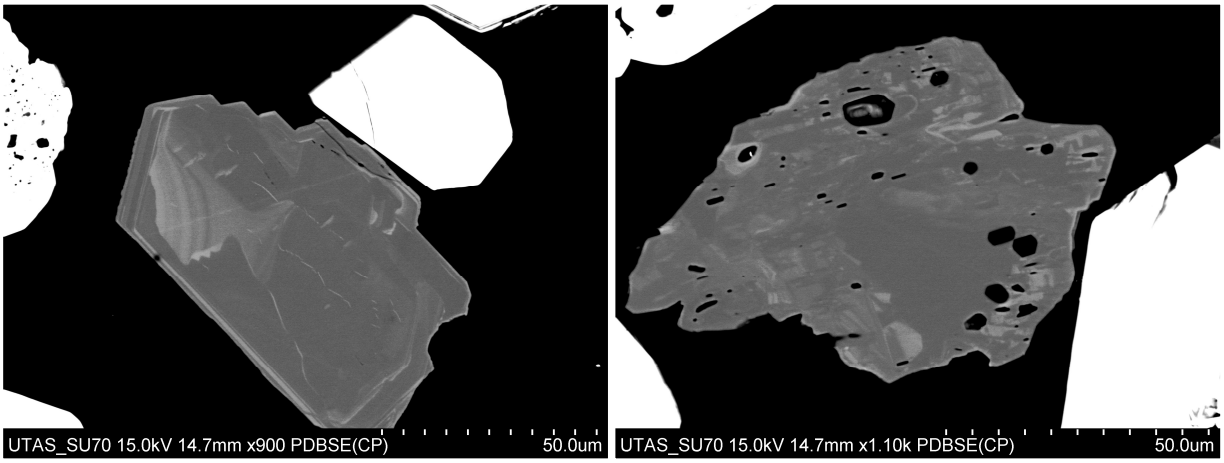


Figure 10. BSE images of examples of highly zoned rutile from the Casino deposit catchment.

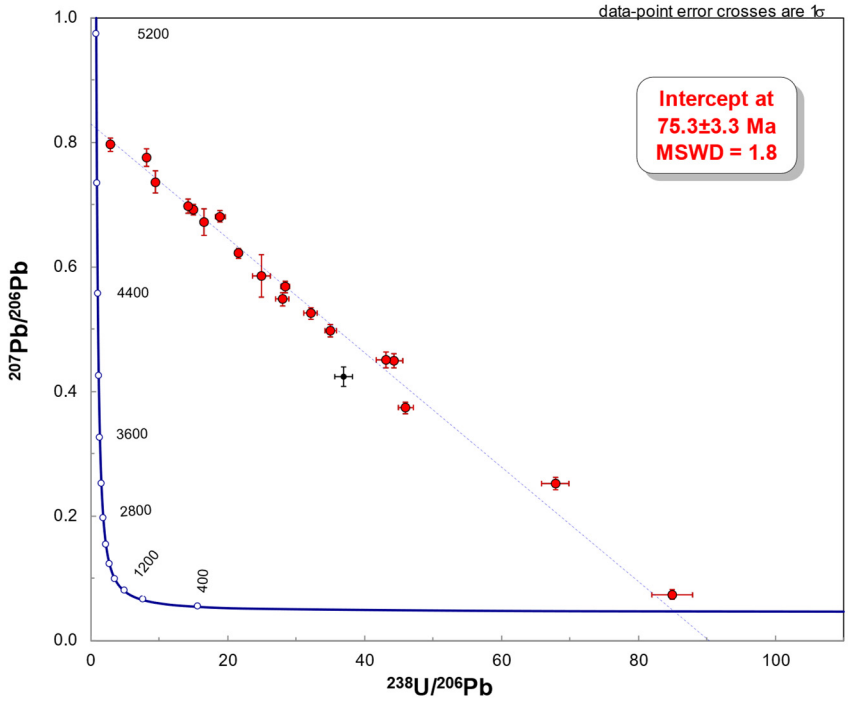


Figure 11. Terra–Wasserburg concordia plot for rutile from a sample within the Casino porphyry Cu deposit catchment with analyses used in calculation highlighted in red.

4.3. Titanite

A total of 312 titanite grains were analysed from 30 samples within the study area (Table S4), with ~35% of them having no age estimate due to very high common Pb

($^{207}Pb/^{206}Pb > 0.8$). The majority of titanite ages are ~260 Ma, with other major age populations at ~160, ~110, ~95, and ~75 Ma (Figure 12a). Titanite is the only mineral analysed that returned a ~95 Ma age corresponding to the formation of the Coffee, Boulevard Au, and Toni Tiger skarn deposits, and is clearly distinguishable from the ~110 Ma age population (Figure 12a).

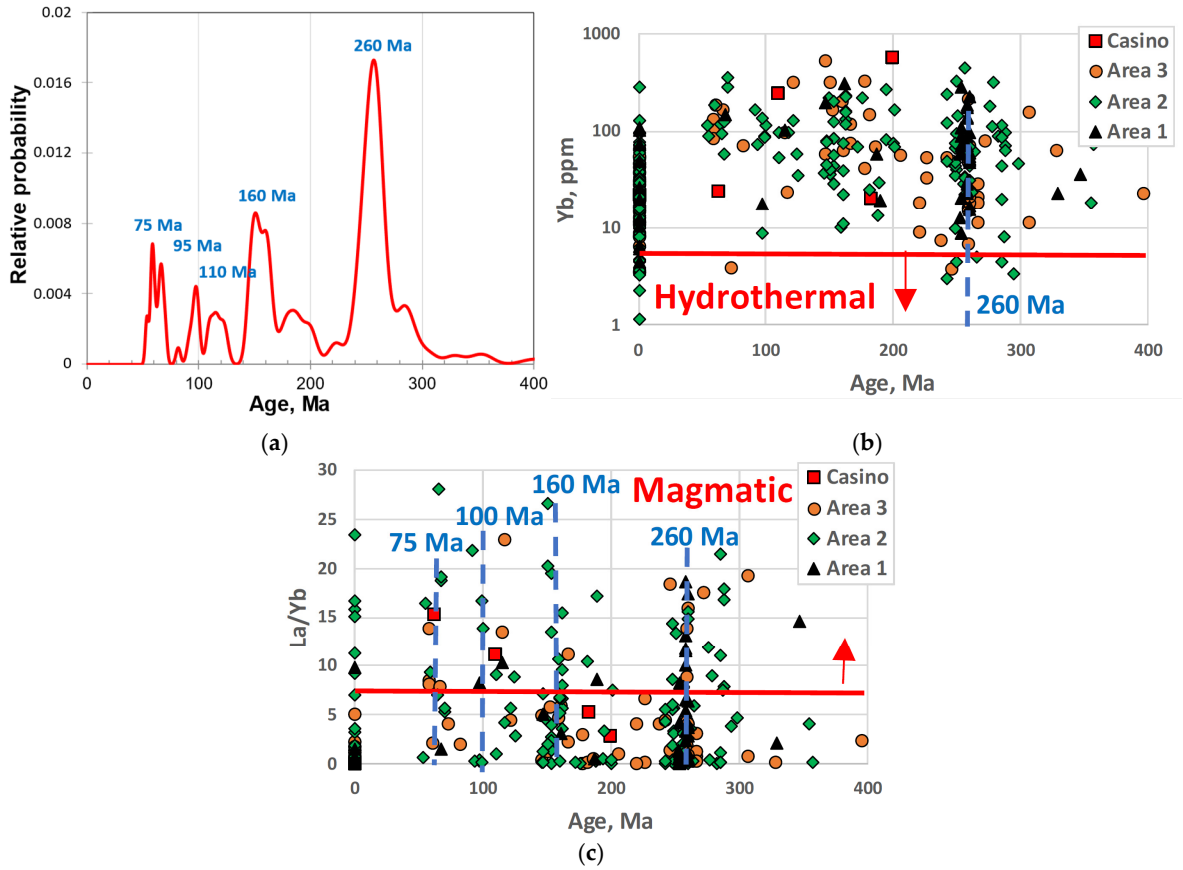


Figure 12. Probability density plot for datable titanites < 400 Ma age from all samples (**a**); compositions of datable rutile showing cutoff for prospective grains used in this study (red horizontal line) shown in (**b**) Yb < 8 ppm (hydrothermal titanite) and (**c**) La/Yb > 7 (magmatic titanite). In (**b**,**c**), grains with no age estimate are shown to have a 0 Ma age.

Hydrothermal titanite. There were 20 titanite grains with low HREE (Yb < 8 ppm). Hydrothermal titanites mostly have low U contents; hence, only ten of them had an age estimate, with nine having ages ~260 Ma and one having a ~70 Ma age (Figure 12b). Catchments of the Casino porphyry Cu and Toni Tiger skarn deposits were not highlighted by hydrothermal titanite (Figure 13a). Most of the prospective hydrothermal titanites come from Area 2 (Figure 12b), where the Coffee Au deposit is located.

Magmatic titanite. There were 61 titanite grains with high LREE/HREE and intermediate HREE (La/Yb > 7, Yb < 200 ppm), with 55 of them having an age estimate. The most prominent age populations in magmatic titanite are ~75 Ma, ~100 Ma, ~160 Ma, and ~260 Ma (Figure 12c). Catchments of the Casino porphyry Cu and Coffee Au deposit were highlighted in terms of their anomalous magmatic titanite chemistry (Figure 13b), but several other catchments dominate the prospective titanite distribution, with ~160 Ma and ~260 Ma age peaks not related to any known mineralisation but possibly related to a fertile signature in basement rocks.

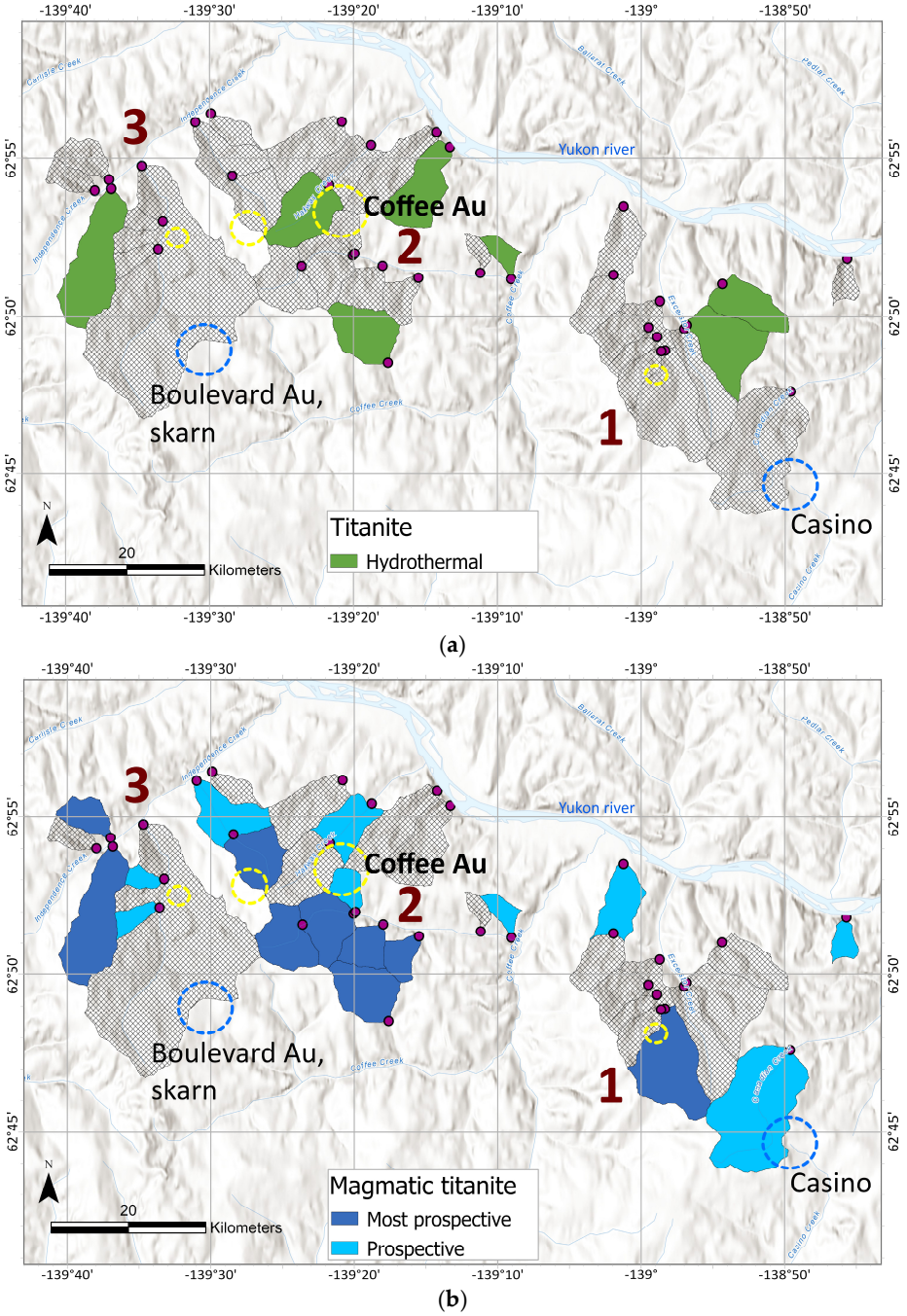


Figure 13. Map showing catchments with the highest number of prospective (**a**) hydrothermal and (**b**) magmatic titanite. Most prospective catchments have the highest proportion of prospective grains. Shaded catchments were sampled but not highlighted by prospectivity criteria. Other symbology from Figure 1.

Catchments adjacent to all deposits within the study area have prospective titanites. The most prospective signature comes from the Central region (Area 2); however, it is marginal to the Coffee Au deposit. Titanites with mostly ~260 and ~160 Ma ages are also abundant; however, they are not related to known mineralisation and possibly reflect the abundance of felsic intrusions in the district. Hydrothermal titanites highlight Area 2, but the majority of them could not be dated due to low U contents.

4.4. Sulfide Indicator Minerals and Scheelite

Additional information can be obtained from the distribution of sulfide minerals and scheelite in the samples. The distribution of chalcopyrite highlights the Casino porphyry Cu deposit catchment and Coffee Au deposit catchments (Figure 14a). Molybdenite distribution highlights the Boulevard Au deposit and Toni Tiger skarn catchments (Figure 14a). Scheelite is widely distributed and is found in the catchments of all deposits in the study area (Figure 14b).

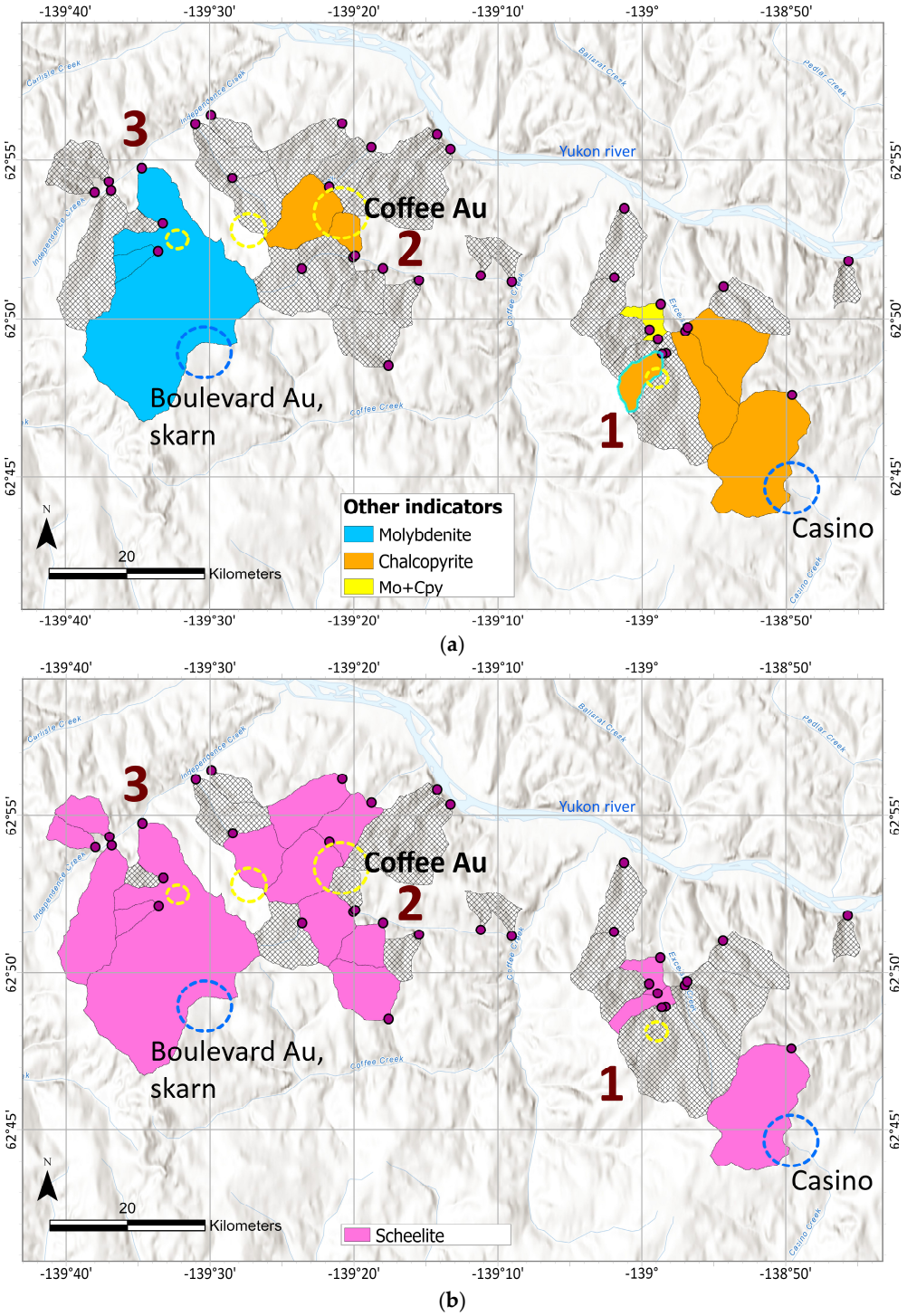


Figure 14. Additional prospectivity indicator minerals in stream sediment samples: (**a**) sulfide mineral distribution; (**b**) scheelite distribution. Shaded catchments were sampled but not highlighted by prospectivity criteria. Other symbology from Figure 1.

4.5. Summaries for Areas

Area 1: Based on heavy mineral chemistry from stream sediments in area 1, we identified this area as the most prospective for porphyry mineralisation. Prospective zircon was mostly ~110 Ma, while the most prospective rutiles were ~75 Ma. Stream sediments from this area also contained chalcopyrite and epidote. The most prospective catchment was the SE one that overlapped with the location of the Casino porphyry deposit.

Area 2: This area was identified as prospective for other styles of mineralisation, possibly intrusion-related or orogenic Au. It has prospective titanite that is mostly ~260 Ma and several catchments with prospective rutile compositions based on Sn, W, Fe, and Nb anomalism. Some chalcopyrite and epidote, as well as widespread scheelite, were found in the area. This area hosts the Coffee Au deposit.

Area 3: This area shows high prospectivity for porphyry and other styles of mineralisation, most likely of Cretaceous age; however, more analyses and dating are required to confirm. Some molybdenite and a few epidote grains were found in samples from the area, as well as widespread scheelite and tourmaline. Prospectivity of the area is confirmed by zircon and rutile compositions (particularly V contents). This area hosts the Boulevard Au deposit and Toni Tiger skarn deposit; however, mineralisation for both is believed to be ~95 Ma [67,69], and few of the minerals dated represent that age of population.

5. Discussion

All the main age peaks identified in different minerals in the area (~340 Ma, ~260 Ma, 160–170 Ma, 95–110 Ma, and ~75 Ma) correspond to a certain geological event. Ore deposits in this area are dominantly hosted within metamorphic rocks of the Yukon–Tanana terrane (YTT) and mid-Cretaceous plutonic rocks. The YTT is a major metamorphic complex in the North American Cordillera, with its primary geological evolution including extensive felsic magmatism occurring during the Late Devonian (~365–340 Ma) [70]. It is a composite terrane containing older basement rocks (>395 Ma) and undergoing a second significant pulse of magmatism in the Middle to Late Permian (~270–250 Ma) [71]. Those basement rocks were intruded by Coffee Creek pluton (~100 Ma) and the Dawson Range batholith (~115–110 Ma), which are both part of the Whitehorse plutonic suite, and a range of late Cretaceous intrusions (70–75 Ma), such as Patton porphyry [59].

The ages of the main mineralisation events in the study area are presented as ~75 Ma for porphyry mineralisation (Casino) [59] and ~95 Ma for orogenic (Coffee and Boulevard) and skarn (Toni Tiger) events [67,69]. Many of the minerals were datable by U/Pb geochronology; however, analyses representing those age populations often have subdued abundance, with the majority of analyses representing minerals from host and basement rocks. Rutile has the most pronounced prospective signature with grains from the catchment of the Casino porphyry Cu deposit producing a 75.3 ± 3.3 Ma age estimate (Figure 11) perfectly matching the established mineralisation age [59].

The sample from the catchment of the Casino porphyry Cu deposit is also highlighted by zircon compositions; however, only one zircon dated from this sample was 75 Ma. The presence of thin rims identified in CL images on these zircons (Figure 6) possibly reflects the timing of the Patton porphyry mineralising event. In most cases, the rims could not be targeted with the 20–30 µm laser ablation spot size used in our analytical method. There is a possibility that the rims were more extensive but eroded during transport. Nevertheless, the catchment shows good prospectivity in terms of zircon compositions, including the presence of fertile signatures in older intrusions with ages mostly reflecting ages of Coffee Creek granite and Dawson Range batholith.

For zircons, few grains show a prospective signature based on their Ce anomaly relative to Eu anomaly (Figure 3), possibly due to apatite co-crystallisation [14], which

was identified in micro-inclusions. The ~110 Ma zircon age population seems to be most prospective, which does not reflect the known age of any mineralisation but possibly highlights the overall fertility of the area.

Few studies have focused on trace element signatures of titanites from different deposit types supported with good-quality data. For example, some studies suggested Ga contents as an indicator of redox conditions; however, in LA-ICP-MS analyses, ^{69}Ga has argide interference from ^{29}Si, which is a major element in titanite, and ^{71}Ga has oxide interference from ^{55}Mn, which can also be quite high in titanites. Therefore, the measurement of low-level Ga can be challenging in titanite, and some of the publications using it might be compromised.

We used low HREE (Yb < 8 ppm) contents as an indicator of fertile hydrothermal titanite compositions. Such compositions only marginally highlight the Coffee deposit (Figure 13a) and are not optimal for U/Pb dating due to low U contents. Magmatic titanites could be identified based on elevated Zr contents (>500 ppm); however, in some cases, titanites contain zircon microinclusions and these data should be treated with care. As an indicator of prospective magmatic titanites, we used high LREE/HREE and intermediate HREE (La/Yb > 7, Yb < 200 ppm). The dominance of the ~260 Ma and ~160 Ma age populations in magmatic titanites (Figure 12a) could be due to older titanites associated with more felsic magmatism dominating the signatures, along with younger hydrothermal titanites not surviving erosion and transport. Nevertheless, magmatic titanites were the only mineral analysed that appeared quite abundant at the ~95 Ma age population (Figure 12a) corresponding to the formation of the Coffee, Boulevard Au, and Toni Tiger skarn deposits. The ~75 Ma age peak corresponding to the age of mineralisation at Casino was also present in titanite data (Figure 12a). Catchments of the Casino porphyry Cu and Coffee Au deposit were highlighted in terms of their anomalous magmatic titanite chemistry, but several other catchments dominated the prospective titanite distribution and possibly relate to other deposit types or the general fertile signature of the area. Rutile was described as a minor phase for Coffee Au deposit [63], but the absence of a ~95 Ma peak in the rutile data might be due to its fine-grained nature.

Rutile mineral chemistry clearly highlights porphyry Cu mineralisation in the district, both in terms of ages and trace element compositions. Elevated Sn and W contents are the best indicators of porphyry Cu mineralisation, while elevated V contents highlight orogenic Au events (Figures 8 and 9). BSE imaging could be used as a cheap screening tool to identify zoned rutiles with high W contents, prospective for porphyry Cu deposit exploration.

The distribution of other minerals, such as sulfides, epidote, and scheelite, is useful in highlighting catchments for follow-up sampling and analysis. The presence of chalcopyrite highlighted the catchments of Casino porphyry and Coffee Au deposits, in addition to the presence of the molybdenite catchment of the Boulevard Au deposit and Toni Tiger skarn deposit. A trace element study of sulfides and scheelite could also be used to complement the selection of most prospective catchments.

Overall, the prospectivity of area 1 is confirmed by the presence of a major porphyry Cu deposit (Casino) and Sugar orogenic Au prospect. Chalcopyrite and epidote are present, while zircon and rutile also show prospective trace element signatures, with rutile from the catchment giving a precise age for the porphyry deposit nearby. The prospectivity of area 2 is related to other styles of mineralisation, as highlighted by the presence of a major orogenic Au deposit (Coffee). Chalcopyrite, epidote, and scheelite are also present in catchments from this area. Titanites show prospective mineral chemistry signatures for orogenic Au mineralisation. The prospectivity of area 3 was also noted, but the low number of samples from the catchments of this area makes it difficult to draw strong conclusions on the prospectivity of specific styles of mineralisation. Some molybdenite,

scheelite, tourmaline, and a few epidote grains were found in stream sediments. Zircon and rutile from this area also showed prospective chemistry but were overall less prospective in their trace element anomalism compared to the other areas of this study.

6. Conclusions

The study was originally developed as a blind test, with the location of the mineral deposits or other mineralisation occurrences not known. Heavy mineral chemistry from stream sediment samples precisely identified the location of mineralisation in the study area and suggested additional targets for follow-up infill sampling. Analysis of zircon and titanite provided insights into a range of formation conditions, from magmatic to hydrothermal; however, most of them were not directly related to known mineralisation in the study area. In this case, rutile worked best for locating the Casino porphyry Cu deposit, while zircon and titanite were also useful in highlighting the overall prospectivity of the area. U/Pb dating of rutile reproduced the mineralisation age of the Casino deposit, while rutile Sn and W concentrations highlighted the catchment containing porphyry Cu mineralisation. Vanadium contents in rutile appear to work better for the identification of catchments related to orogenic Au mineralisation. Other possible targets could be identified using mineralogical information from this study. The distribution of sulfides and scheelite are useful in highlighting catchments for follow-up sampling and analysis.

This study highlights that the addition of trace element mineral chemistry and U/Pb geochronology analyses to an exploration program provides benefits in terms of constraining the age of basement and host rocks and prioritising targets. Heavy mineral chemistry from stream sediments used for regional-scale targeting and followed up by rock chip sampling and analysis at the camp scale can provide significant exploration results, as demonstrated in this study. The choice of minerals that are used should depend on the geology of the area, metamorphic overprint, presence of the cover, and deposit type. In this case, rutile was most useful; however, in other cases, zircon and titanite can be equally or more important. BSE imaging of rutile is useful in highlighting presence of zones high in W indicative of proximity to porphyry Cu mineralisation, while CL imaging of zircon is required in order not to miss the thin rims present on some of the grains.

Supplementary Materials: The following supporting information can be downloaded at https://www.mdpi.com/article/10.3390/min16030237/s1. Table S1: Sample coordinates; Table S2: Compositions of zircons; Table S3: Compositions of rutile; Table S4: Compositions of titanites.

Author Contributions: Conceptualisation, I.B., M.J.B., L.D. and J.B.; methodology, I.B., M.J.B. and L.D.; formal analysis, I.B. and M.J.B.; investigation, I.B. and M.J.B.; data curation, I.B. and M.J.B.; writing—original draft preparation, I.B.; writing—review and editing, I.B., M.J.B. and L.D.; visualisation, I.B.; supervision, L.D.; project administration, L.D.; funding acquisition, L.D. All authors have read and agreed to the published version of the manuscript.

Funding: This research was funded by the AMIRA P1202 project.

Data Availability Statement: All compositional and geochronological data for zircon, rutile, and titanite are located in the Supplementary Material.

Acknowledgments: We would like to thank David Cooke for the acquisition of funding and help with project administration; Francisco Testa, Lejun Zhang, and Emily Smyk are thanked for their help with sample preparation and SEM, in addition to Maxwell Morissette for his help with LA-ICP-MS analyses and Karsten Goemann for his help with EPMA/SEM. Reviews from four anonymous reviewers substantially improved the manuscript.

Conflicts of Interest: The co-authors Leonid Danyushevsky and Jeffrey Bigelow are affiliated with the companies Friendly Solutions and Newmont Corporation, respectively. The remaining authors

declare that the research was conducted in the absence of any commercial or financial relationships that could be construed as a potential conflict of interest.

References

1. Gurney, J.; Zweistra, P. The interpretation of the major-element compositions of mantle minerals in diamond exploration. *J. Geochem. Explor.* **1995**, *53*, 293–309. [CrossRef]
2. Grutter, H.S.; Gurney, J.J.; Menzies, A.H.; Winter, F. An updated classification scheme for mantle-derived garnet, for use by diamond explorers. *Lithos* **2004**, *77*, 841–857. [CrossRef]
3. Sobolev, N.; Lavrent'ev, Y.G.; Pokhilenko, N.; Usova, L. Chrome-rich garnets from kimberlites of Yakutia and their parageneses. *Contrib. Mineral. Petrol.* **1973**, *40*, 39–52.
4. Griffin, W.; Ryan, C. Trace-elements in indicator minerals—Area selection and target evaluation in diamond exploration. *J. Geochem. Explor.* **1995**, *53*, 311–337. [CrossRef]
5. Barnes, S.J.; Roeder, P.L. The range of spinel compositions in terrestrial mafic and ultramafic rocks. *J. Petrol.* **2001**, *42*, 2279–2302. [CrossRef]
6. Wyatt, B.; Baumgartner, M.; Anckar, E.; Grutter, H. Compositional classification of "kimberlitic" and "non-kimberlitic" ilmenite. *Lithos* **2004**, *77*, 819–840. [CrossRef]
7. Grütter, H. Pyroxene xenocryst geotherms: Techniques and application. *Lithos* **2009**, *112*, 1167–1178. [CrossRef]
8. Thompson, J.; Meffre, S.; Maas, R.; Kamenetsky, V.; Kamenetsky, M.; Goemann, K.; Ehrig, K.; Danyushevsky, L. Matrix effects in Pb/U measurements during LA-ICP-MS analysis of the mineral apatite. *J. Anal. At. Spectrom.* **2016**, *31*, 1206–1215. [CrossRef]
9. Jenkins, K.; Goemann, K.; Belousov, I.; Morissette, M.; Danyushevsky, L. Investigation of the ablation behaviour of andradite-grossular garnets and rutile with implications for U-Pb geochronology. *Geostand. Geoanal. Res.* **2023**, *47*, 267–295. [CrossRef]
10. Storey, C.D.; Smith, M.P.; Jeffries, T.E. In situ LA-ICP-MS U-Pb dating of metavolcanics of Norrbotten, Sweden: Records of extended geological histories in complex titanite grains. *Chem. Geol.* **2007**, *240*, 163–181. [CrossRef]
11. Guillong, M.; Wotzlaw, J.; Looser, N.; Laurent, O. Evaluating the reliability of U-Pb laser ablation inductively coupled plasma mass spectrometry (LA-ICP-MS) carbonate geochronology: Matrix issues and a potential calcite validation reference material. *Geochronology* **2020**, *2*, 155–167. [CrossRef]
12. Schirra, M.; Laurent, O. Petrochronology of hydrothermal rutile in mineralized porphyry Cu systems. *Chem. Geol.* **2021**, *581*, 120407. [CrossRef]
13. Hogmalm, K.; Zack, T.; Karlsson, A.; Sjöqvist, A.; Garbe-Schönberg, D. In situ Rb-Sr and K-Ca dating by LA-ICP-MS/MS: An evaluation of N_2O and SF_6 as reaction gases. *J. Anal. At. Spectrom.* **2017**, *32*, 305–313. [CrossRef]
14. Loader, M.A.; Wilkinson, J.J.; Armstrong, R.N. The effect of titanite crystallisation on Eu and Ce anomalies in zircon and its implications for the assessment of porphyry Cu deposit fertility. *Earth Planet. Sci. Lett.* **2017**, *472*, 107–119. [CrossRef]
15. Nathwani, C.L.; Loader, M.A.; Wilkinson, J.J.; Buret, Y.; Sievwright, R.H.; Hollings, P. Multi-stage arc magma evolution recorded by apatite in volcanic rocks. *Geology* **2020**, *48*, 323–327. [CrossRef]
16. Scott, K.M. Rutile geochemistry as a guide to porphyry Cu-Au mineralization, Northparkes, New South Wales, Australia. *Geochem. Explor. Environ. Anal.* **2005**, *5*, 247–253. [CrossRef]
17. Pacey, A.; Wilkinson, J.J.; Cooke, D.R. Chlorite and epidote mineral chemistry in porphyry ore systems: A case study of the Northparkes district, New South Wales, Australia. *Econ. Geol.* **2020**, *115*, 701–727. [CrossRef]
18. Wilkinson, J.; Chang, Z.; Cooke, D.; Baker, M.; Wilkinson, C.; Inglis, S.; Chen, H.; Gemmell, J. The chlorite proximitor: A new tool for detecting porphyry ore deposits. *J. Geochem. Explor.* **2015**, *152*, 10–26. [CrossRef]
19. Lee, R.G.; Plouffe, A.; Ferbey, T.; Hart, C.J.R.; Hollings, P.; Gleeson, S.A. Recognizing porphyry copper potential from till zircon composition: A case study from the Highland Valley porphyry district, south-central British Columbia. *Econ. Geol.* **2021**, *116*, 1035–1045. [CrossRef]
20. Cooke, D.R.; Agnew, P.; Hollings, P.; Baker, M.; Chang, Z.S.; Wilkinson, J.J.; Ahmed, A.; White, N.C.; Zhang, L.J.; Thompson, J.; et al. Recent advances in the application of mineral chemistry to exploration for porphyry copper-gold-molybdenum deposits: Detecting the geochemical fingerprints and footprints of hypogene mineralization and alteration. *Geochem. Explor. Environ. Anal.* **2020**, *20*, 176–188. [CrossRef]
21. Von Eynatten, H.; Dunkl, I. Assessing the sediment factory: The role of single grain analysis. *Earth-Sci. Rev.* **2012**, *115*, 97–120. [CrossRef]
22. Chew, D.; O'Sullivan, G.; Caracciolo, L.; Mark, C.; Tyrrell, S. Sourcing the sand: Accessory mineral fertility, analytical and other biases in detrital U-Pb provenance analysis. *Earth-Sci. Rev.* **2020**, *202*, 103093. [CrossRef]
23. Thompson, J.M.; Meffre, S.; Danyushevsky, L. Impact of air, laser pulse width and fluence on U-Pb dating of zircons by LA-ICPMS. *J. Anal. At. Spectrom.* **2018**, *33*, 221–230. [CrossRef]

24. Jochum, K.P.; Weis, U.; Stoll, B.; Kuzmin, D.; Yang, Q.C.; Raczek, I.; Jacob, D.E.; Stracke, A.; Birbaum, K.; Frick, D.A.; et al. Determination of reference values for NIST SRM 610–617 glasses following ISO guidelines. *Geostand. Geoanal. Res.* **2011**, *35*, 397–429. [CrossRef]
25. Wiedenbeck, M.; Alle, P.; Corfu, F.; Griffin, W.; Meier, M.; Oberli, F.; Vonquadt, A.; Roddick, J.; Speigel, W. 3 natural zircon standards for U-Th-Pb, Lu-Hf, trace-element and REE analyses. *Geostand. Newsl.* **1995**, *19*, 1–23. [CrossRef]
26. Thompson, J.; Goemann, K.; Belousov, I.; Jenkins, K.; Kobussen, A.; Powell, W.; Danyushevsky, L. Assessment of the mineral ilmenite for U-Pb dating by LA-ICP-MS. *J. Anal. At. Spectrom.* **2021**, *36*, 1244–1260. [CrossRef]
27. Baker, J.; Peate, D.; Waight, T.; Meyzen, C. Pb isotopic analysis of standards and samples using a Pb-207–Pb-204 double spike and thallium to correct for mass bias with a double-focusing MC-ICP-MS. *Chem. Geol.* **2004**, *211*, 275–303. [CrossRef]
28. Black, L.; Kamo, S.; Allen, C.; Aleinikoff, J.; Davis, D.; Korsch, R.; Foudoulis, C. Temora 1: A new zircon standard for Phanerozoic U-Pb geochronology. *Chem. Geol.* **2003**, *200*, 155–170. [CrossRef]
29. Sláma, J.; Kosler, J.; Condon, D.; Crowley, J.; Gerdes, A.; Hanchar, J.; Horstwood, M.; Morris, G.; Nasdala, L.; Norberg, N.; et al. Plesovice zircon: A new natural reference material for U-Pb and Hf isotopic microanalysis. *Chem. Geol.* **2008**, *249*, 1–35. [CrossRef]
30. Luvizotto, G.; Zack, T.; Meyer, H.; Ludwig, T.; Triebold, S.; Kronz, A.; Münker, C.; Stockli, D.; Prowatke, S.; Klemme, S.; et al. Rutile crystals as potential trace element and isotope mineral standards for microanalysis. *Chem. Geol.* **2009**, *261*, 346–369. [CrossRef]
31. Zack, T.; Stockli, D.; Luvizotto, G.; Barth, M.; Belousova, E.; Wolfe, M.; Hinton, R. In situ U-Pb rutile dating by LA-ICP-MS: 208Pb correction and prospects for geological applications. *Contrib. Mineral. Petrol.* **2011**, *162*, 515–530. [CrossRef]
32. Schmitz, M.; Bowring, S. U-Pb zircon and titanite systematics of the Fish Canyon Tuff: An assessment of high-precision U-Pb geochronology and its application to young volcanic rocks. *Geochim. Cosmochim. Acta* **2001**, *65*, 2571–2587. [CrossRef]
33. Schoene, B.; Bowring, S. U-Pb systematics of the McClure Mountain syenite: Thermochronological constraints on the age of the 40Ar/39Ar standard MMhb. *Contrib. Mineral. Petrol.* **2006**, *151*, 615–630. [CrossRef]
34. Chew, D.; Petrus, J.; Kamber, B. U-Pb LA-ICPMS dating using accessory mineral standards with variable common Pb. *Chem. Geol.* **2014**, *363*, 185–199. [CrossRef]
35. Horstwood, M.; Kosler, J.; Gehrels, G.; Jackson, S.; McLean, N.; Paton, C.; Pearson, N.; Sircombe, K.; Sylvester, P.; Vermeesch, P.; et al. Community-derived standards for LA-ICP-MS U-(Th-)Pb geochronology—Uncertainty propagation, age interpretation and data reporting. *Geostand. Geoanal. Res.* **2016**, *40*, 311–332. [CrossRef]
36. Ballard, J.; Palin, J.; Campbell, I. Relative oxidation states of magmas inferred from Ce(IV)/Ce(III) in zircon: Application to porphyry copper deposits of northern Chile. *Contrib. Mineral. Petrol.* **2002**, *144*, 347–364. [CrossRef]
37. Dilles, J.H.; Kent, A.J.R.; Wooden, J.L.; Tosdal, R.M.; Koleszar, A.; Lee, R.G.; Farmer, L.P. Zircon compositional evidence for sulfur-degassing from ore-forming arc magmas. *Econ. Geol.* **2015**, *110*, 241–251. [CrossRef]
38. Lu, Y.-J.; Loucks, R.R.; Fiorentini, M.; McCuaig, T.C.; Evans, N.J.; Yang, Z.-M.; Hou, Z.-Q.; Kirkland, C.L.; Parra-Avila, L.A.; Kobussen, A.; et al. Zircon compositions as a pathfinder for porphyry Cu ± Mo ± Au deposits. In *Tectonics and Metallogeny of the Tethyan Orogenic Belt*; Society of Economic Geologists: Littleton, CO, USA, 2016; Volume 19.
39. Ahmed, A. *Epidote and Chlorite Mineral Chemistry from the Yerington Porphyry Copper District, USA: Genetic and Exploration Implications*; University of Tasmania: Hobart, Australia, 2019.
40. Loucks, R.R.; Fiorentini, M.L.; Henriquez, G.J. New magmatic oxybarometer using trace elements in zircon. *J. Petrol.* **2020**, *61*, egaa034. [CrossRef]
41. Porter, J.K.; McNaughton, N.J.; Evans, N.J.; McDonald, B.J. Rutile as a pathfinder for metals exploration. *Ore Geol. Rev.* **2020**, *120*, 103406. [CrossRef]
42. Scibiorski, E.; Cawood, P. Titanite as a petrogenetic indicator. *Terra Nova* **2022**, *34*, 177–183. [CrossRef]
43. Gros, K.; Slaby, E.; Birski, L.; Kozub-Budzyn, G.; Sláma, J. Geochemical evolution of a composite pluton: Insight from major and trace element chemistry of titanite. *Mineral. Petrol.* **2020**, *114*, 375–401. [CrossRef]
44. Hu, H.; Li, J.; McFarlane, C.; Luo, Y.; McCarron, T. Textures, trace element compositions, and U-Pb ages of titanite from the Mangling granitoid pluton, East Qinling Orogen: Implications for magma mixing and destruction of the North China Craton. *Lithos* **2017**, *284*, 50–68. [CrossRef]
45. McLeod, G.; Dempster, T.; Faithfull, J. Deciphering magma-mixing processes using zoned titanite from the Ross of Mull Granite, Scotland. *J. Petrol.* **2011**, *52*, 55–82. [CrossRef]
46. Laurent, O.; Zeh, A.; Gerdes, A.; Villaros, A.; Gros, K.; Slaby, E. How do granitoid magmas mix with each other? Insights from textures, trace element and Sr-Nd isotopic composition of apatite and titanite from the Matok pluton (South Africa). *Contrib. Mineral. Petrol.* **2017**, *172*, 80. [CrossRef]
47. Hayden, L.A.; Watson, E.B.; Wark, D.A. A thermobarometer for sphene (titanite). *Contrib. Mineral. Petrol.* **2008**, *155*, 529–540. [CrossRef]

48. Kohn, M.J. Titanite petrochronology. In *Petrochronology: Methods and Applications*; Kohn, M.J., Engi, M., Lanari, P., Eds.; Reviews in Mineralogy & Geochemistry, Volume 83; Mineralogical Society of America and Geochemical Society: Chantilly, VA, USA, 2017; pp. 419–441.
49. Mottram, C.; Cottle, J.; Kylander-Clark, A. Campaign-style U-Pb titanite petrochronology: Along-strike variations in timing of metamorphism in the Himalayan metamorphic core. *Geosci. Front.* **2019**, *10*, 827–847. [CrossRef]
50. Spencer, K.; Hacker, B.; Kylander-Clark, A.; Andersen, T.; Cottle, J.; Stearns, M.; Poletti, J.; Seward, G. Campaign-style titanite U-Pb dating by laser-ablation ICP: Implications for crustal flow, phase transformations and titanite closure. *Chem. Geol.* **2013**, *341*, 84–101. [CrossRef]
51. Hart-Madigan, L.; Wilkinson, J.J.; Lasalle, S.; Armstrong, R.N. U-Pb dating of hydrothermal titanite resolves multiple phases of propylitic alteration in the Oyu Tolgoi porphyry district, Mongolia. *Econ. Geol.* **2020**, *115*, 1605–1618. [CrossRef]
52. Aleinikoff, J.; Wintsch, R.; Fanning, C.; Dorais, M. U-Pb geochronology of zircon and polygenetic titanite from the Glastonbury Complex, Connecticut, USA: An integrated SEM, EMPA, TIMS, and SHRIMP study. *Chem. Geol.* **2002**, *188*, 125–147. [CrossRef]
53. Pan, L.; Hu, R.; Bi, X.; Li, C.; Wang, X.; Zhu, J. Titanite major and trace element compositions as petrogenetic and metallogenic indicators of Mo ore deposits: Examples from four granite plutons in the southern Yidun arc, SW China. *Am. Mineral.* **2018**, *103*, 1417–1434. [CrossRef]
54. Cao, M.; Qin, K.; Li, G.; Evans, N.; Jin, L. In situ LA-(MC)-ICP-MS trace element and Nd isotopic compositions and genesis of polygenetic titanite from the Baogutu reduced porphyry Cu deposit, Western Junggar, NW China. *Ore Geol. Rev.* **2015**, *65*, 940–954. [CrossRef]
55. Adam, J.; Green, T.H.; Sie, S.H. Proton microprobe determined partitioning of Rb, Sr, Ba, Y, Zr, Nb and Ta between experimentally produced amphiboles and silicate melts with variable F content. *Chem. Geol.* **1993**, *109*, 29–49. [CrossRef]
56. Migdisov, A.; Williams-Jones, A.; Brugger, J.; Caporuscio, F. Hydrothermal transport, deposition, and fractionation of the REE: Experimental data and thermodynamic calculations. *Chem. Geol.* **2016**, *439*, 13–42. [CrossRef]
57. Xu, L.; Bi, X.; Hu, R.; Tang, Y.; Wang, X.; Xu, Y. LA-ICP-MS mineral chemistry of titanite and the geological implications for exploration of porphyry Cu deposits in the Jinshajiang–Red River alkaline igneous belt, SW China. *Mineral. Petrol.* **2015**, *109*, 181–200. [CrossRef]
58. Selby, D.; Creaser, R.; Nesbitt, B. Major and trace element compositions and Sr-Nd-Pb systematics of crystalline rocks from the Dawson Range, Yukon, Canada. *Can. J. Earth Sci.* **1999**, *36*, 1463–1481. [CrossRef]
59. Selby, D.; Creaser, R. Late and mid-Cretaceous mineralization in the northern Canadian Cordillera: Constraints from Re-Os molybdenite dates. *Econ. Geol.* **2001**, *96*, 1461–1467. [CrossRef]
60. McClenaghan, M.; Beckett-Brown, C.; McCurdy, M.; Casselman, S. Stream sediment indicator mineral signatures of the Casino porphyry Cu-Au-Mo deposit, Yukon, Canada. *Econ. Geol.* **2023**, *118*, 411–431. [CrossRef]
61. Beckett-Brown, C.; McDonald, A.; McClenaghan, M.; McCurdy, M. Evaluating the application of texture and chemistry of detrital tourmaline as an indicator of porphyry Cu mineralization: A case study from the Casino porphyry Cu-Au-Mo deposit, Yukon, Canada. *J. Geochem. Explor.* **2024**, *262*, 107469. [CrossRef]
62. Kidder, J.; McClenaghan, M.; Leybourne, M.; McCurdy, M.; Pelchat, P.; Layton-Matthews, D.; Voinot, A. Hydrogeochemistry of porphyry-related solutes in ground and surface waters; an example from the Casino Cu-Au-Mo deposit, Yukon, Canada. *Geochem. Explor. Environ. Anal.* **2022**, *22*, geochem2021-058. [CrossRef]
63. MacWilliam, K. The Geology and Genesis of the Coffee Gold Deposit in West-Central Yukon, Canada: Implications for the Structural, Magmatic, and Metallogenic Evolution of the Dawson Range, and Gold Exploration Models. Ph.D. Thesis, The University of British Columbia, Vancouver, BC, Canada, 2018; p. 497.
64. Buitenhuis, E. The Latte Gold Zone, Kaminak's Coffee Gold Project, Yukon, Canada: Geology, Geochemistry, and Metallogeny. Master's Thesis, University of Western Ontario, London, ON, Canada, 2014.
65. Allan, M.; Mortensen, J.; Hart, C.; Bailey, L.; Sanchez, M.; Ciolkiewicz, W.; McKenzie, G.; Creaser, R. Magmatic and metallogenic framework of west-central Yukon and eastern Alaska. In *SEG Special Publication*; Society of Economic Geologists: Littleton, CO, USA, 2013; Volume 17, pp. 111–168.
66. MacKenzie, D.; Craw, D.; Finnigan, C. Lithologically controlled invisible gold, Yukon, Canada. *Mineral. Deposita* **2015**, *50*, 141–157. [CrossRef]
67. McKenzie, G. Geology and Mineralization at Independence Creek: Dawson Range, West-Central Yukon Territory. Master's Thesis, The University of British Columbia, Vancouver, BC, Canada, 2014.
68. Bartlett, S. Geology, Alteration, and Mineralization of the Sugar Gold Prospect, Yukon Territory, Canada. Bachelor's Thesis, The University of British Columbia, Vancouver, BC, Canada, 2016; p. 76.
69. Well-Shen, L. A Petrographic and Fluid Inclusion Comparison of Mid-Cretaceous Gold Bearing Veins near the 5 Moz Coffee Deposit, West-Central Yukon. Bachelor's Thesis, The University of British Columbia, Vancouver, BC, Canada, 2017.

70. La Roche, R.; Zagorevski, A.; Joyce, N.; Crowley, J. Paleozoic evolution of the Yukon-Tanana terrane of the North American Cordillera, NW British Columbia. *Geosphere* **2024**, *20*, 476–504. [CrossRef]
71. Mortensen, J. Pre-mid-Mesozoic tectonic evolution of the Yukon-Tanana terrane, Yukon and Alaska. *Tectonics* **1992**, *11*, 836–853. [CrossRef]

Disclaimer/Publisher's Note: The statements, opinions and data contained in all publications are solely those of the individual author(s) and contributor(s) and not of MDPI and/or the editor(s). MDPI and/or the editor(s) disclaim responsibility for any injury to people or property resulting from any ideas, methods, instructions or products referred to in the content.